Effects of aggregation and electron injection on photovoltaic performance of porphyrin-based solar cells with oligo(phenylethynyl) links inside TiO_2 and Al_2O_3 nanotube arrays†

Liyang Luo,[ab] Chia-Jung Lin,[a] Chiau-Yiag Tsai,[a] Hui-Ping Wu,[a] Lu-Lin Li,[a] Chen-Fu Lo,[c] Ching-Yao Lin[c] and Eric Wei-Guang Diau*[a]

Received 24th September 2009, Accepted 4th November 2009
First published as an Advance Article on the web 2nd December 2009
DOI: 10.1039/b919962d

Porphyrins with phenylethynyl links of varied length (PE1–PE4) were sensitized on vertically oriented, anodic titanium-oxide (ATO) nanotube arrays for application as dye-sensitized solar cells (DSSC). The efficiency of power conversion decreased systematically from the dye with a short link to the dye with a long link. We measured the efficiency of conversion of incident photons to current (IPCE), the photocurrent decay of the devices, and steady-state and time-resolved fluorescence spectra of the thin-film samples to understand how the cell performance depends on the length of the link. Measurements of femtosecond fluorescence confirmed that the efficiency of electron injection depended on length because of dye aggregation that significantly increased the rate of aggregate-induced energy transfer for porphyrins with a long link. The rate of electron injection depended on the length of the link with an attenuation factor $\beta \sim 0.1$ Å^{-1}. Resonant energy transfer (RET) kinetics of porphyrins sensitized on anodic aluminium-oxide (AAO) nanotube arrays were performed with picosecond time-correlated single-photon counting and four molecular densities for each porphyrin. The kinetic data of PE1 and PE2 are described satisfactorily according to a Förster model, whereas those of PE3 and PE4 conform to a Dexter formula. A formation of clusters is proposed to rationalize the observed density-dependent kinetics for the RET of porphyrins on semiconductor films.

1. Introduction

Dye-sensitized solar cells (DSSC) have attracted much attention in relation to global warming and the search for cheap and effective sources of renewable energy.[1] The overall efficiency (η) of power conversion of a DSSC is controlled by the primary processes—electron injection, charge recombination, dye regeneration and electron collection at the electrode.[2] Charge separation occurs initially in the dye upon irradiation; electrons subsequently proceed to the interface between the dye and TiO_2 through a bridge or link. Careful design of the structure of the dye with appropriate links can thus minimize the rate of charge recombination, to improve the cell performance.[3] The design of various links that spatially separate the dye chromophore and TiO_2 provides a model system for fundamental investigation. For flexible links, the insertion of saturated –CH_2– groups into the dye significantly diminished the coupling of electrons between the dye and TiO_2, leading to a markedly decreased rate of electron injection.[4] For rigid links, Galoppini and co-workers[5] reported that the rates of bi-exponential electron injection in the Ru-bpy/TiO_2 system decreased with increasing length of the rigid π-conjugated phenylethynyl (PE) links. To enhance our understanding of the role of a linker with respect to the efficiency of a DSSC, we have designed zinc porphyrins, with the length of the link controlled by the number of PE units, for a porphyrin with one PE unit (denoted PE1) up to a porphyrin with four PE units (PE4),[6] as shown in Chart 1.

With PE1–PE4 sensitized on nanocrystalline TiO_2 films to make nanoparticle (NP)-based DSSC devices, the efficiency, η, of power conversion decreases systematically with increasing length of the link, which was not interpretable according to the rate of electron injection independent of length.[6c] Further investigation of the dynamics using femtosecond (fs) transient absorption revealed that the porphyrin with a long link (PE4)

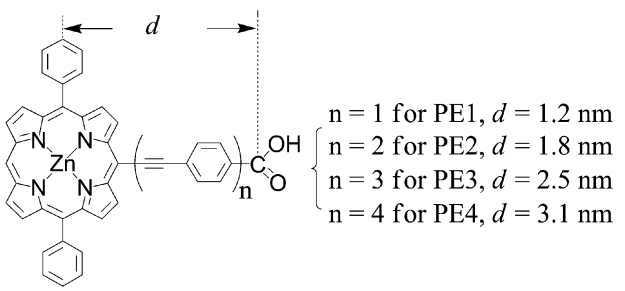

Chart 1

[a] *Department of Applied Chemistry and Institute of Molecular Science, National Chiao Tung University, Hsinchu 300, Taiwan. E-mail: diau@mail.nctu.edu.tw*
[b] *Institute of Chemistry, Academia Sinica, Taipei, Taiwan*
[c] *Department of Applied Chemistry, National Chi Nan University, Puli, Nantou Hsien, Taiwan*

† Electronic supplementary information (ESI) available: Summary of photovoltaic properties (Table S1), SEM images of ATO and AAO films (Fig. S1), and the theoretical fits of the femtosecond transients (Table S2 and Fig. S2 and S3). See DOI: 10.1039/b919962d

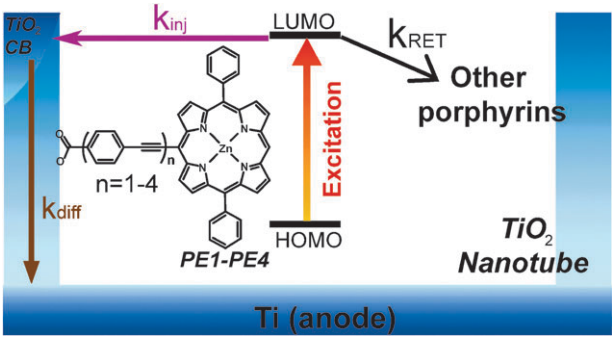

Fig. 1 A schematic representation to illustrate the key processes involved in a porphyrin-based NT-DSSC device.

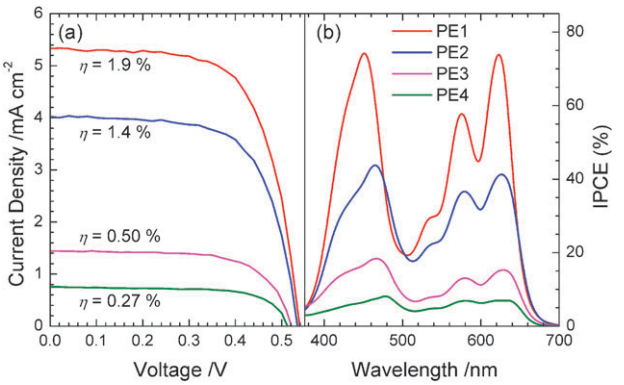

Fig. 2 (a) Current–voltage characteristics of NT-DSSC devices with sensitizers PE1–PE4 collected under AM1.5 1-sun illumination (100 mW cm^{-2}), calibrated with a Si-based reference cell; the corresponding photovoltaic parameters are summarized in Table S1, ESI.† (b) Corresponding action spectra of conversion efficiency of incident photons to current (IPCE) of PE1–PE4; the active cell area is 0.25 cm^2.

has more rapid back-transfer of electrons (BET) than a porphyrin with a short link (PE1), indicating that BET might occur more efficiently through space in a randomly packed mesoporous environment such as a TiO_2 NP film.[6d] To avoid the possibility of BET through space, in the present work we used vertically aligned arrays of anodic titanium-oxide (ATO) nanotubes (NT) as the electron-transport layer to fabricate the NT-DSSC devices[7] with PE1–PE4 as sensitizers. Fig. 1 illustrates the fundamental electron transfer and energy transfer processes involved in a porphyrin-based NT-DSSC device. To understand the cell performance of these porphyrins depending on the length of the PE link, we measured the photovoltaic and transient photocurrents of these devices, as well as the fluorescence decays of the corresponding porphyrin-sensitized ATO NT and anodic aluminium oxide (AAO) NT films (Fig. S1, ESI†) on femtosecond or picosecond time scales.

2. Results and discussion

2.1 Photovoltaic performance

Fig. 2a shows the photovoltaic characteristics of four porphyrin-based DSSC devices fabricated with identical ATO films with NT of length ~15 μm. Like their NP-counterparts,[6c] the efficiencies of power conversion of these NT-DSSC devices decreased systematically from 1.9% (PE1), 1.4% (PE2), 0.50% (PE3) to 0.27% (PE4). The corresponding photovoltaic parameters are summarized in Table S1, ESI.† This systematic variation of the cell performance is best indicated by the short-circuit photocurrent density (J_{SC}), which decreased from 5.3 mA cm^{-2} (PE1) to 0.75 mA cm^{-2} (PE4) as the length of the PE link increased from d = 1.2 nm to 3.1 nm. Fig. 2b shows action spectra for the efficiency of conversion of incident photons to current (IPCE) for the same devices of which the I–V characteristics are shown in Fig. 2a. These IPCE values exhibit a systematic decrease from PE1 to PE4. Our results again demonstrate that the cell performance depends directly on the length of a rigid π-conjugated link: the longer the link, the poorer the cell performance becomes. This conclusion is the same as what we found for PE1–PE4 in NP-DSSC devices,[6c] but the speculated BET through space[6d] is impracticable for porphyrins sensitized inside nanotubes. We thus exclude the BET through space as a key process to account for the observed length-dependent performance of the porphyrin-based DSSC.

2.2 Laser-induced photocurrent decays

We applied pulsed laser-induced photocurrent transients[8] to measure the kinetics of electron transport of the NT-DSSC devices after electron injection from porphyrins under AM 1.5 one-sun illumination. The experimental setup is displayed in Fig. 3. The ns-pulsed laser (EKSPLA, NT342) generated an excitation pulse at 435 nm (1 mW, FWHM ~8 ns); the resulting photocurrent at the short-circuit condition (ΔI_{SC}) after passing a low-noise current preamplifier (Stanford Research Systems, SR570) was collected with an oscilloscope.

Fig. 4 shows ΔI_{SC} transients for the same devices as those for photovoltaic properties shown in Fig. 2. We observed a systematic variation of the ΔI_{SC} decay of PE1–PE4, for which the electron transport under the short-circuit condition systematically slowed with increasing length of the link from PE1 to PE4. The observed decay of the photocurrent of devices PE1–PE4 reflects only the transport of electrons on the TiO_2 surface of the ATO films with the same quality; the rates of diffusion are strongly correlated with the length of the

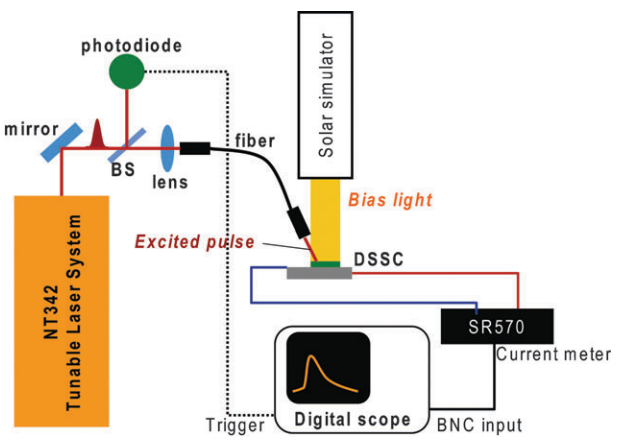

Fig. 3 Experimental setup for measurement of photocurrent decay.

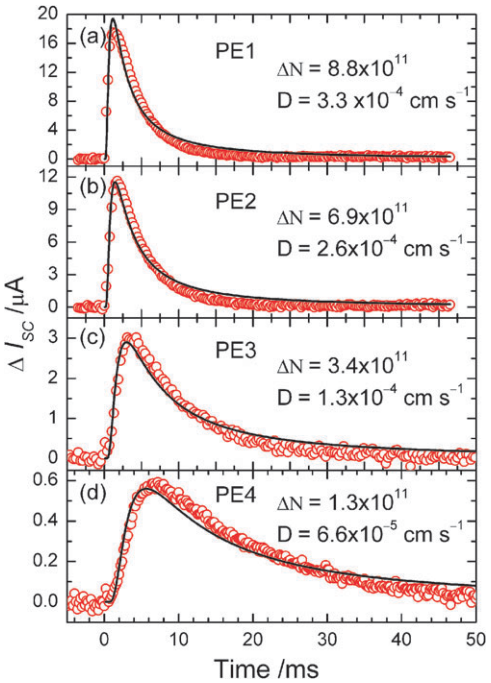

Fig. 4 Photocurrent transients of the corresponding devices obtained with pulse excitation at 430 nm under constant bias light of one-sun AM1.5 irradiation. The transient data (circles) were fitted according to a diffusion kinetic model formulated in eqn (1).

link upon neglect of charge recombination under short-circuit conditions. To understand the diffusion character of the transients, we fitted decays, ΔI_{SC}, with an equation for diffusion current depending on time:[9]

$$\Delta I_{SC}(t) = \frac{qW\Delta N}{2\sqrt{\pi D}t^{3/2}} e^{-W^2/4Dt} \quad (1)$$

in which appear film thickness (W = 15 μm), number of photoelectrons, ΔN, and diffusion coefficient D.

Fig. 4 shows the fitted results (black curves) for PE1–PE4 according to eqn (1); the slight discrepancy between the data and the fitted curves is due to insufficient parameters in the simple diffusion kinetic model applied here. Nevertheless, the rise and decay in the photocurrent transients can be understood to be due to the effect of diffusion of the electrons on ATO films, taking trapping and de-trapping into account. The values of $D/10^{-4}$ cm^{-1} systematically decreased from 3.3 (PE1), 2.6 (PE2), 1.3 (PE3) to 0.66 (PE4). The amplitudes of the transients are characterized with ΔN (of order 10^{11}), which also decreased systematically from 8.8 (PE1), 6.9 (PE2), 3.4 (PE3), to 1.3 (PE4). The electrons of PE4 on ATO NT arrays numbered one seventh of those of PE1, which reasonably accounts for J_{SC} decreasing to one seventh from PE1 to PE4. We hence conclude that the degradation of the cell performance from PE1 to PE4 was due to the reduction of the conduction-band electrons (ΔN) on the ATO film, which shows a systematically decreasing trend from a short link (PE1) to a long link (PE4). This phenomenon can be understood through investigation of the time-resolved fluorescence.

2.3 Absorption and fluorescence spectra

The results for the transient photocurrent show that the conduction-band electrons injected from PE4 were fewer than those injected from PE1, implying that the yield of electron injection (Φ_{inj}) is much smaller for the former than for the latter. To estimate Φ_{inj} for the system, we measured steady-state and time-resolved fluorescence for PE1–PE4 sensitized on ATO and AAO films of the same quality. The amounts of dye loading on each semiconductor film for each porphyrin were made to be as similar as possible, implemented by adjusting the appropriate dye-soaking period for each film; the absorption spectra of the sensitized semiconductor films of PE1–PE4 are shown in Fig. 5a–d, respectively. Fig. 6a and b show fluorescence spectra of porphyrin-sensitized AAO and ATO films, respectively. For PE1–PE4 sensitized on AAO films, the fluorescence spectra show the mirror images of the Q band of the absorption spectra (Fig. 5), and the fluorescence intensities decreased systematically from PE1 to PE4 (Fig. 6a). On ATO films, the emissions were significantly quenched with the intensity order PE4 > PE3 > PE2 > PE1 (Fig. 6b). Note that the fluorescence intensities of the ATO films are much lower than those of the AAO films and the spectral shape of the ATO films deviates from the AAO films due to the involvement of electron injection in the ATO films. Therefore, we might assign the origin of the emission spectra of the ATO films to be the vibrationally hot porphyrin species in the first electronic excited state (S_1), whereas the emissions of the AAO films originate from the cold S_1 state as in the case of porphyrins in solution.[6c] We emphasize that these results imply two important points: aggregate-induced energy transfer plays an important role to account for fluorescence quenching of the porphyrin-sensitized AAO films, such that the effect of quenching is more pronounced when the porphyrin has a long link to facilitate ππ-stacking aggregation on the AAO surface. When porphyrins were sensitized on ATO films, not only the aggregation, but also the interfacial electron transfer, are involved in the observed fluorescence quenching on an ATO surface. The rapid electron injection produces further quenching of fluorescence with the rate of injection in the sequence PE1 > PE2 > PE3 > PE4.

2.4 Femtosecond fluorescence decays

With fs fluorescence decays, we investigated the dynamics of interfacial electron injection in the porphyrin/ATO films; the porphyrin/AAO films served as reference for the aggregation-only condition. We performed fs excitation of the thin-film samples at 430 nm using a fluorescence up-conversion system described elsewhere.[6a] The emissions at 620 nm were optically gated with the fundamental pulse (860 nm) to yield the emission decays of PE1–PE4, shown in Fig. 7. All fs transients are characterized with two decay components with those of the AAO films involving an additional slow-decay component; the fitted decay coefficients are summarized in Table S2, ESI.† Note that the decay coefficients are much slower than those obtained from their NP-counterparts,[6c] because the porphyrins might aggregate more significantly on nanoparticles than inside the nanotubes. Under such a condition, we are able to extract the length-dependent electron-injection yields from

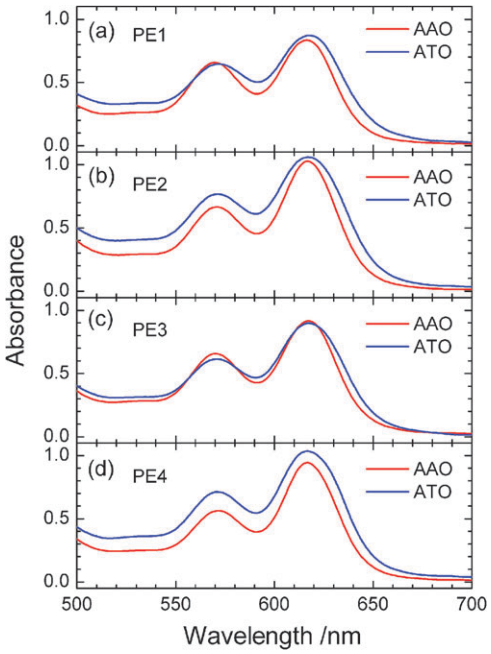

Fig. 5 Absorption spectra of AAO and ATO films sensitized with (a) PE1, (b) PE2, (c) PE3 and (d) PE4 for measurements of femtosecond fluorescence decay.

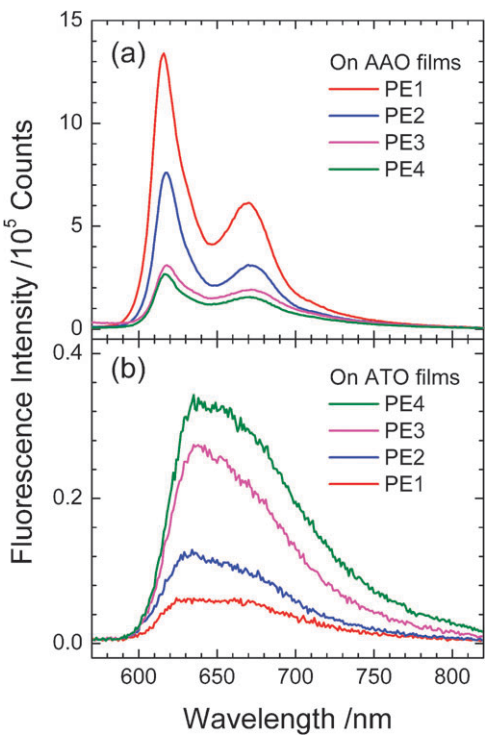

Fig. 6 Steady-state fluorescence spectra of PE1–PE4 sensitized on (a) AAO films and (b) ATO films.

analyzing the observed fs kinetics of the sensitized ATO and AAO films. With the time coefficients weighted by their relative amplitudes, the average time coefficients of the ATO films are 0.9, 1.4, 2.0 and 2.4 ps for PE1, PE2, PE3, and PE4, respectively; and those of the AAO films are 70, 21, 4.5 and 2.4 ps,

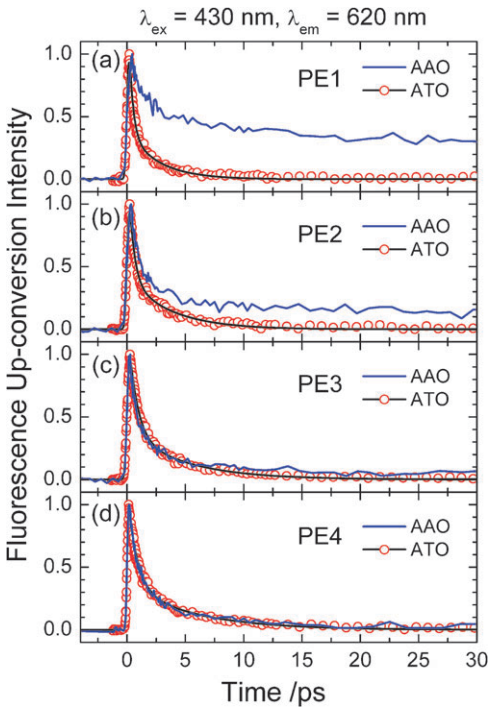

Fig. 7 Corresponding femtosecond fluorescence transients of PE1–PE4 sensitized films with excitation at 430 nm and emission at 620 nm; raw data were fitted according to an appropriate kinetic model (Table S2, Fig. S2 and S3, ESI†).

respectively. The emission decays of the AAO films reflect only intermolecular energy transfer due to aggregation of the dye on the Al_2O_3 surface, but the emission decays of the ATO films contain not only the aggregate-induced energy transfer, but also rapid electron injection from the excited state of a porphyrin into the conduction band of TiO_2. If we assume that the extent of dye aggregation on both ATO and AAO films is similar, based on the same amount of dye molecules adsorbed on the films (Fig. 5) with similar nanostructural morphology, the quantum yields for electron injection of PE1, PE2, PE3 and PE4 on the TiO_2 surface become evaluated to be Φ_{inj} = 0.99, 0.93, 0.56 and ~0, respectively. Φ_{inj} of PE4 was nearly zero because the large contribution of aggregate-induced energy transfer overwhelmed the interfacial electron transfer so that an accurate rate of electron injection of PE4 could not be obtained. Nevertheless, that the decrease of Φ_{inj} depends on the length of the link is understood as reflecting both significant aggregation and slower injection for the long link.

Using fs transient absorption, Galoppini and coworkers tested a Ru-complex model system with the PE link varying from one to three units, similar to our PE1–PE3 cases;[5] they similarly found that the kinetics of electron injection of the complexes bound to TiO_2 exhibit a bi-exponential feature. A plot of rate coefficients for electron injection as a function of d for the Ru-bpy/TiO_2 system yielded an attenuation β-factor of 0.04 Å^{-1}, indicating a weak correlation of electron transfer with the length of the link.[5] For our porphyrin/ATO-NT system, the average time coefficients of electron injection are 0.9, 1.5, and 3.5 ps for PE1–PE3 respectively, *i.e.*, the electron injection decreased to a quarter when the distance doubled.

This nature of distance attenuation is described with an exponential decay and a β-factor of 0.1 $Å^{-1}$, which is larger than that of the Ru-bpy/TiO_2 system of Galoppini and coworkers[5] but smaller than that of a porphyrin-based donor–bridge–accepter system that has a β-factor of 0.20 $Å^{-1}$, determined according to a Förster model of energy transfer.[10]

2.5 Resonance energy transfer (RET)

Our fs results indicate that the efficiencies of electron injection of the porphyrin-sensitized ATO films depend strongly on the length of the link because porphyrins aggregate inside the nanotubes. To derive information regarding the effect of porphyrin aggregation, we investigated the ps relaxation kinetics using time-correlated single-photon counting (TCSPC), detailed elsewhere,[11] for various densities of PE1–PE4 sensitized inside AAO NT. The control of the molecular densities of porphyrins on AAO films was achieved by soaking films of the size ~2.8 cm^2 into porphyrin/ethanol solutions (volume = 3.0 mL) of four concentrations in ~30 min. Fig. 8a–d show the differential absorption spectra of PE1–PE4 in ethanol, respectively, with four ΔA (optical path length = 1 mm) on each plot representing the varied absorbances of the solutions before and after immersion of the AAO films. With the total surface area of the AAO films being estimated to be 1.35×10^3 cm^2, and the absorption coefficients ($\varepsilon/10^4$ cm^{-1} M^{-1}) of PE1–PE4 being known to be 2.6, 4.0, 3.6, and 3.4, respectively, the amounts of dye-loading on the surface of the AAO films can thus be evaluated in the range of (0.7–4.8) × 10^{13} molecules cm^{-2} for each porphyrin (Table 1). Assuming that the porphyrins were evenly adsorbed on the AAO surface, the averaged distance (r) of the molecules can be estimated to be in the range of 1.4–3.9 nm (Table 1).

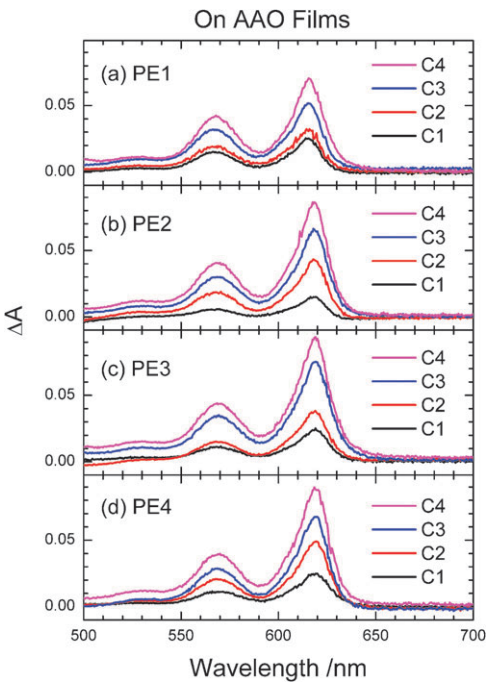

Fig. 8 Difference of absorption spectra between before and after immersion of identical AAO films into four concentrations (labeled as C1–C4) of (a) PE1, (b) PE2, (c) PE3, and (d) PE4; the corresponding spectral and dye-loading parameters are summarized in Table 1.

Fig. 9a–d show the ps fluorescence decays of the AAO films sensitized with PE1–PE4, respectively; the amounts of dye loading are determined from the corresponding results shown in Fig. 8a–d. The transients are satisfactorily characterized with two decay components (τ_1 and τ_2); the fitted time coefficients and the corresponding relative amplitudes are summarized in Table 1. We found three general features of the observed relaxation kinetics. First, the values of τ_1 depend strongly on the molecular densities (or r) for each porphyrin, and the fluorescence decays are more rapid when the average molecular distances are smaller. Second, the values of τ_2 are less dependent on r and they are smaller than those observed in the corresponding solutions.[6c] Third, the relative amplitudes are less sensitive to r for PE1 and PE2 but they become highly dependent on r for PE3 and PE4; in particular, the rapid-decay component became a predominant part of the transient for PE3 and PE4 at greater densities. Because energy transfer occurred between the same molecules, the slow-decay component plays a role as an energy sink, whereas the excitation energy is propagated (rapid-decay component). After quantitatively analyzing our kinetic data using an appropriate model (see below), we propose a mechanism of energy transfer induced by aggregates to account for the observed relaxation kinetics: the rapid-decay component (τ_1) is due to resonant energy transfer (RET) from an excited molecule to a ground-state species; the slow-decay component (τ_2) is assigned to electronic relaxation that is responsible for the observed fluorescence quenching upon dye aggregation.

The rate coefficient (k_T) of RET is described according to this Förster formula,[12–14]

$$k_T = \frac{1}{\tau_D}\left(\frac{R_0}{r}\right)^6 \qquad (2)$$

in which τ_D is the relaxation coefficient of an isolated donor molecule in the excited state; in our case, τ_D = 1.9 ns for PE1 and τ_D = 2.1 ns for PE2–PE4.[6c] τ_D represents the time coefficient of RET occurring at distance r between the excited-state porphyrin (donor) and the ground-state porphyrin (acceptor) equal to Förster radius, R_0. Hence, R_0 is a critical distance at which RET and spontaneous decay of the excited porphyrin are equally likely. For a typical donor–acceptor system of organic molecules, R_0 is in the range 2–6 nm.[13] With this background in mind, we examined our kinetic data for the RET rate coefficient ($k_T = \tau_1^{-1}$) as a function of r^{-6}; the results appear in Fig. 10a.

The experimental data deviate from the theoretical model with two features. First, the plots of k_T*versus* r^{-6} exhibit linearity for PE1 and PE2, but not for PE3 and PE4; another model should be considered for the latter case. Second, the theoretical fits of PE1 and PE2 fail to intersect the origin; *i.e.*, k_T was not equal to zero as r approaches infinity. An expression modified from eqn (2) was applied to fit our RET kinetic data:

$$k_T = k_0 + \frac{1}{\tau_0}\left(\frac{R_0}{r}\right)^6 \qquad (3)$$

Table 1 Spectral parameters to estimate the average distance (r) and kinetic parameters to evaluate the rate coefficient for resonant energy transfer (k_1).[a,b]

Species	Concentration[c]	A_{film}	ΔA	DL[d]	r/nm	τ_1 (A_1)/ns	τ_2 (A_2)/ns	k_1[e]/10^9 s^{-1}	k_2[e]/10^9 s^{-1}
PE1	C1	0.47	0.025	1.73	2.40	0.37 (0.49)	1.2 (0.51)	2.7	0.85
	C2	0.66	0.028	1.93	2.28	0.34 (0.45)	1.2 (0.55)	3.0	0.86
	C3	0.80	0.052	3.59	1.67	0.29 (0.51)	1.1 (0.49)	3.4	0.93
	C4	0.94	0.070	4.83	1.44	0.25 (0.53)	1.0 (0.47)	4.0	1.02
PE2	C1	0.34	0.015	0.67	3.86	0.34 (0.37)	1.2 (0.63)	2.9	0.83
	C2	0.57	0.043	1.92	2.28	0.26 (0.45)	1.1 (0.55)	3.9	0.88
	C3	0.87	0.065	2.90	1.86	0.24 (0.46)	1.1 (0.54)	4.2	0.92
	C4	1.15	0.086	3.83	1.62	0.15 (0.63)	1.0 (0.37)	6.8	1.04
PE3	C1	0.37	0.024	1.17	2.92	0.34 (0.40)	1.2 (0.60)	3.0	0.82
	C2	0.65	0.038	1.86	2.32	0.22 (0.50)	1.1 (0.50)	4.6	0.92
	C3	0.91	0.075	3.67	1.65	0.10 (0.59)	1.1 (0.41)	10.1	0.87
	C4	1.27	0.094	4.59	1.48	0.08 (0.78)	0.9 (0.22)	12.4	1.08
PE4	C1	0.34	0.025	1.31	2.76	0.13 (0.57)	1.4 (0.43)	7.5	0.73
	C2	0.66	0.048	2.51	2.00	0.09 (0.67)	1.2 (0.33)	11.3	0.86
	C3	0.95	0.067	3.51	1.69	0.08 (0.81)	1.1 (0.19)	12.8	0.93
	C4	1.25	0.089	4.66	1.46	0.07 (0.87)	1.0 (0.13)	13.7	1.00

[a] Spectral parameters measured at 620 nm; values of ΔA from Fig. 8 and those of A_{film} from reflectance spectra using a spectrophotometer (JASCO, V-570) with an integrating sphere (ISN-470). [b] Kinetic parameters (relative amplitudes shown in parentheses) obtained from theoretical fits of the fluorescence decay curves shown in Fig. 9. [c] The same concentration labels as shown in Fig. 8 and 9. [d] Dye loading density in unit 10^{13} cm^{-2}. [e] Rate coefficients converted from the reversal of the corresponding time coefficients.

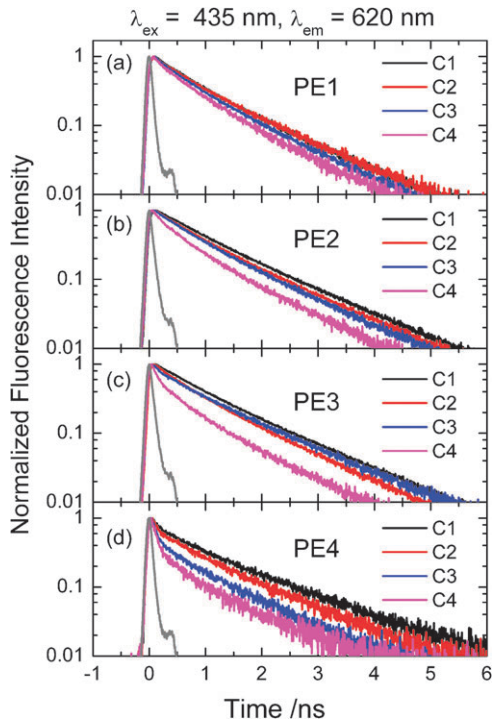

Fig. 9 Corresponding picosecond fluorescence transients of the same sensitized AAO samples as those shown in Fig. 8; the fitted kinetic parameters are summarized in Table 1.

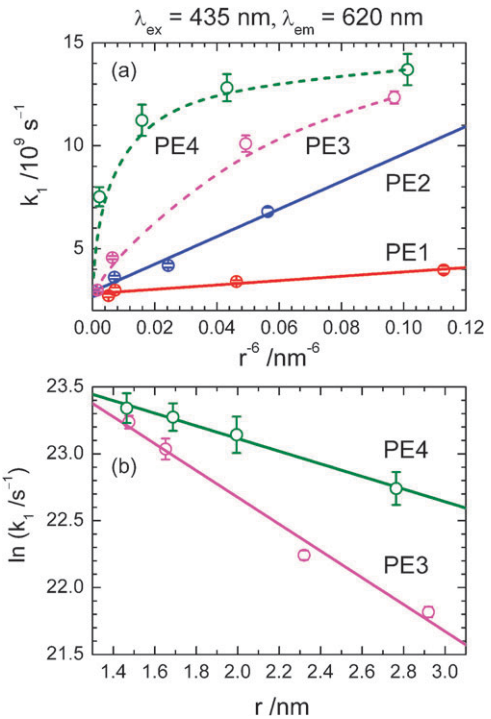

Fig. 10 (a) RET rate coefficient (k_1) *vs.* r^{-6} for PE1–PE4 sensitized on AAO films; the solid straight lines are the theoretical fits according to Förster's formula, eqn (3). (b) ln k_1 *vs.* r for PE3 and PE4 sensitized on AAO flims; the straight lines are theoretical fits according to Dexter's formula, eqn (4).

in which k_0 ($=\tau_0^{-1}$) represents the RET rate coefficient under a limiting dilute condition, so that the average distance between donor and acceptor tends to zero. As shown in Fig. 10a, the kinetic data of PE1 and PE2 were fitted satisfactorily according to eqn (3), yielding an intercept of $k_0/10^9$ s^{-1} = 2.8 and a slope of $\frac{R_0^6}{\tau_0}/10^9\,s^{-1}\,nm^6 = 11$ for PE1, but 2.9 and 71 for PE2, respectively. The existence of a non-zero intercept ($k_0 \sim 3 \times 10^9$ s^{-1}) implies two possibilities. First, the isolated excited molecule interacts with the AAO surface so that the transfer of the excitation energy occurred at the interface between the porphyrin and AAO. k_0 thus represents the relaxation coefficient of the corresponding single-molecular interfacial energy transfer at the limiting condition (r = 0). Under such a condition, R_0 is evaluated as 1.3 and 1.7 nm for PE1 and PE2, respectively. Second, the porphyrin molecules might form small aggregated

clusters on the surface of AAO films at a limiting dilute condition. In this case, k_0 represents an intrinsic rate coefficient for the relaxation of the excited porphyrin cluster unit formed inside the AAO NT, and the average distance between the porphyrin clusters should become modified to nr; n is the number of porphyrins forming a cluster. Accordingly, the Förster critical radius should also become modified to nR_0 within this model. Judging from: (i) the values of k_0 are similar for both PE1 and PE2 (the interaction between porphyrin and AAO should depend on the length of the PE link in this case); (ii) the values of R_0 estimated from the first case are smaller than those of the large organic molecules, which are well determined ($R_0 \sim 6$ nm),[13] the second possibility is more likely to properly describe the RET model for what we have observed with a cluster size estimated to be $n \sim 5$.

Because the Förster critical radius involves several photophysical parameters,[13] which are similar for PE1 and PE2, the discrepancy of R_0 between PE1 and PE2 might reflect the orientation factor, κ^2. In principle, κ^2 can be in a range from 0 (perpendicular orientation), 1 (parallel orientation) to 4 (collinear orientation).[13] We therefore expect that the larger orientation factor of PE2 *vs.* PE1 is due to the rigidity of the molecules, for which the porphyrins were originally aligned on the surface of the AAO nanotubes in a parallel fashion ($\kappa^2 \sim 1$). The molecules with link PE2 would have more freedom to adopt a tilted head-to-tail geometry ($1 < \kappa^2 < 4$) than those of link PE1, so that a larger κ^2 value, and thus a larger R_0 value, is expected for PE2 than for PE1. For the case of PE3 and PE4, the plots of k_T*versus* r^{-6} show even steeper slopes (dashed curves shown in Fig. 10a), indicating that the values of κ^2 are large for long links, so that the flexibility toward head-to-tail orientation depends on the length of the link. The kinetic data of PE3 and PE4 cannot, however, be fitted satisfactorily according to eqn (3), because the traditional long-range dipole–dipole RET model failed to describe a heavily aggregated system, such as PE3 and PE4. We therefore resort to an exchange mechanism for the RET rate coefficient (k_T^{ex}), expressible according to Dexter's formula:[13,14]

$$k_T^{ex} = KJ \exp(-2r/L) \quad (4)$$

in which K denotes a constant, J is the integral overlap between the donor (absorption) and the acceptor (emission), and L is the average Bohr radius that characterizes the size of the interaction in the exchange mechanism.

Fig. 10b shows plots of $\ln(k_T^{ex})$ *versus* r for PE3 and PE4; the corresponding straight lines are fitted results according to eqn (4). The kinetic data exhibit linearity with L/nm determined to be 2.0 and 4.3 for PE3 and PE4, respectively. That L of PE4 is larger than that of PE3 is understood to be due to the tighter aggregation for PE4 than for PE3. The size of L seems, however, to be too large relative to values reported for other porphyrins ($L = 0.48$ nm),[14] and the critical distance for the RET of porphyrins on switching from the Förster to the Dexter mechanism was estimated to be 0.5–0.6 nm.[14] As discussed earlier, we assigned the observed kinetics to reflect a RET between porphyrin clusters for PE1 and PE2 based on the Förster model. For data analysis based on the Dexter formulation for PE3 and PE4, we speculate that the observed kinetics might be due to a RET inside the clusters, so that the correction for L becomes L/n'. In this way the number of porphyrins in the clusters (n') of PE3 and PE4 might be similar to that of PE1 and PE2 ($n' \cong n \sim 5$). More experimental evidence should be provided to illustrate the RET model proposed here, and it would also require more theoretical effort to consolidate the two models applied for RET of porphyrins on the surface of semiconductors.

3. Conclusion

We report the photovoltaic performance of a porphyrin/ATO-NT system with the π-conjugated link of porphyrins varying from one PE unit (PE1) to four PE units (PE4). Transient photocurrent measurements indicate that the number of free electrons and the corresponding diffusion coefficients decrease systematically from PE1 to PE4, so to account for the length-dependent cell performance of the system. Steady-state and time-resolved fluorescence measurements of the ATO and AAO films confirm that an aggregate-induced energy transfer is the key factor to be considered for the smaller yield of electron injection resulting from the greater ππ-stacking aggregation of the porphyrins with a long PE link. The rate of electron injection depends on the length of the link (for PE1–PE3), with a distance attenuation factor $\beta \sim 0.1$ Å^{-1}; the rate of energy transfer that depends on the extent of aggregation is described with Förster (for PE1 and PE2) or Dexter (for PE3 and PE4) formulae, based on a cluster-formation model. Our results thus indicate that the design of porphyrins with bulky or long-chain groups in PE links of moderate length to avoid dye aggregation is effective for promoting cell performance for future porphyrin-based DSSC.

4. Experiments

4.1 Preparation of AAO and ATO nanochannel array films

AAO and ATO thin-film samples were fabricated through standard procedures described elsewhere.[7,15] The AAO samples were made with 3 vol% oxalic acid ($C_2H_2O_4$, 99%) at 40 V and 20 °C. As pores are randomly created on the AAO surface, a regular pattern is obtained when AAO is removed by wet chemical etching using a mixture of 6 mass % phosphoric acid (H_3PO_4, 98%) and 1.8 mass % chromic oxide (CrO_3, 95%) at 60 °C for 40 min. After a second anodization for 4 h under the same conditions, the AAO nano-channel arrays grew based on these patterns.

We fabricated ordered nanochannel arrays of ATO films at 25 °C on anodizing titanium foil (Aldrich, 99.7%) as circular discs (diameter 50 mm) at a constant potential of 60 V with anodization for various periods.[7] The electrolyte solution contained ammonium fluoride in ethylene glycol in the presence of water. To crystallize amorphous TiO_2 into an anatase phase, we annealed the samples to 450 °C. Ultrasonic vibration removes the unwanted deposits from the surface ATO. Fig. S1a and b (ESI)† show SEM images of ATO and AAO nano-channel arrays with pore sizes of 80 and 100 nm, respectively.

4.2 Device fabrication

To characterize the photovoltaic performance of the NT-DSSC devices, we immersed the ATO films (active size 0.4 × 0.4 cm^2) in a THF solution containing PE1–PE4 (1×10^{-4} M) at 40 °C for 3 h to adsorb sufficient porphyrin molecules to harvest light; the porphyrin/ATO films served as a working electrode (anode). A fluorine-doped tin oxide (FTO; 30 Ω/sq, Sinonar, Taiwan) glass (typical size 1.0 × 2.0 cm^2) sputtered with Pt particles served as a counter electrode (cathode). To fabricate the NT-DSSC device, we assembled the two electrodes into a cell of sandwich type and sealed it with a hot-melt film (SX1170, Solaronix, thickness 25 μm); a thin layer of electrolyte was introduced into the space between the two electrodes. A typical electrolyte contained LiI (0.1 M), I_2 (0.01 M), 4-*t*-butylpyridine (TBP, 0.5 M), butyl methyl imidazolium iodide (BMII, 0.6 M), and guanidinium thiocyanate (GuNCS, 0.1 M) in a mixture of acetonitrile (CH_3CN, 99.9%) and valeronitrile (n-C_4H_9CN, 99.9%) (v/v) 15/1).

4.3 Photovoltaic characterization

The current–voltage characteristics were determined with a digital source meter (Keithley 2400, computer-controlled) with the device under one-solar AM 1.5 irradiation from a solar simulator (SAN-EI, XES-502S) calibrated with a standard silicon reference cell (VLSI standards, Oriel PN 91150V). The spectra of the efficiency of conversion of incident photons to current (IPCE) of the corresponding devices were recorded with a system comprising a Xe lamp (PTi A–1010, 150 W), a monochromator (Dongwoo DM150i, 1200 gr/mm blazed at 500 nm), and a source meter (Keithley 2400). A standard Si photodiode (ThorLabs FDS1010) served as a reference to calibrate the power density of the light source at each wavelength.[7]

Acknowledgements

National Science Council of Taiwan and Ministry of Education of Taiwan, under the ATU program, provided support for this project.

References

1 (*a*) M. Grätzel, *Nature*, 2001, **414**, 338; (*b*) M. Grätzel, *Inorg. Chem.*, 2005, **44**, 6841.
2 (*a*) T. W. Hamann, R. A. Jensen, A. B. F. Martinson, H. V. Ryswyk and J. T. Hupp, *Energy Environ. Sci.*, 2008, **1**, 66; (*b*) A. B. F. Martinson, T. W. Hamann, M. J. Pellin and J. T. Hupp, *Chem.–Eur. J.*, 2008, **14**, 4458.
3 (*a*) K. Kilsa, E. I. Mayo, D. Kuciauska, R. Villahermosa, N. S. Lewis, J. R. Winkler and H. B. Gray, *J. Phys. Chem. A*, 2003, **107**, 3379; (*b*) E. Galoppini, *Coord. Chem. Rev.*, 2004, **248**, 1283; (*c*) J. R. Stromberg, A. Marton, H. L. Kee, C. Kirmaier, J. R. Diers, C. Muthiah, M. Taniguchi, J. S. Lindsey, D. F. Bocian, G. J. Meyer and D. Holten, *J. Phys. Chem. C*, 2007, **111**, 15464; (*d*) J. Rochford, D. Chu, A. Hagfeldt and E. Galoppini, *J. Am. Chem. Soc.*, 2007, **129**, 4655; (*e*) J. Rochford and E. Galoppini, *Langmuir*, 2008, **24**, 5366; (*f*) N. R. de Tacconi, W. Chanmanee, K. Rajeshwar, J. Rochford and E. Galoppini, *J. Phys. Chem. C*, 2009, **113**, 2996.
4 (*a*) N. A. Anderson and T. Lian, *Coord. Chem. Rev.*, 2004, **248**, 1231; (*b*) N. A. Anderson and T. Lian, *Annu. Rev. Phys. Chem.*, 2005, **56**, 491.
5 M. Myahkostupov, P. Piotrowiak, D. Wang and E. Galoppini, *J. Phys. Chem. C*, 2007, **111**, 2827.
6 (*a*) L. Luo, C.-F. Lo, C.-Y. Lin, I.-J. Chang and E. W.-G. Diau, *J. Phys. Chem. B*, 2006, **110**, 410; (*b*) C.-F. Lo, L. Luo, E. W.-G. Diau, I.-J. Chang and C.-Y. Lin, *Chem. Commun.*, 2006, 1430; (*c*) C.-Y. Lin, C.-F. Lo, L. Luo, H.-P. Lu, C.-S. Hung and E. W.-G. Diau, *J. Phys. Chem. C*, 2009, **113**, 755; (*d*) C.-W. Chang, L. Luo, C.-K. Chou, C.-F. Lo, C.-Y. Lin, C.-S. Hung, Y.-P. Lee and E. W.-G. Diau, *J. Phys. Chem. C*, 2009, **113**, 11524.
7 C.-C. Chen, H.-W. Chung, C.-H. Chen, H.-P. Lu, C.-M. Lan, S.-F. Chen, L. Luo, C.-S. Hung and E. W.-G. Diau, *J. Phys. Chem. C*, 2008, **112**, 19151.
8 N. W. Duffy, L. M. Peter and K. G. U. Wijayantha, *Electrochem. Commun.*, 2000, **2**, 262.
9 A. Solbrand, H. Lindström, H. Rensmo, A. Hagfeldt, S.-E. Lindquist and S. Södergren, *J. Phys. Chem. B*, 1997, **101**, 2514.
10 K. Pettersson, A. Kyrychenko, E. Rönnow, T. Ljungdahl, J. Mårtensson and B. Albinsson, *J. Phys. Chem. A*, 2006, **110**, 310.
11 L. Luo, C.-H. Chang, Y.-C. Chen, T.-K. Wu and E. W.-G. Diau, *J. Phys. Chem. B*, 2007, **111**, 7656.
12 (*a*) Th. Förster, *Ann. Phys.*, 1948, **437**, 55; (*b*) Th. Förster, *Disc. Far. Soc.*, 1959, **7**, 17.
13 B. Valeur, *Molecular Fluorescence: Principles and Applications*, Wiley-VCH, New York, USA, 2002.
14 S. Faure, C. Stern, R. Guilard and P. D. Harvey, *J. Am. Chem. Soc.*, 2004, **126**, 1253.
15 (*a*) J.-S. Lin, Y.-C. Chen, C.-C. Chen, E. W.-G. Diau and T.-F. Liu, *J. Chin. Chem. Soc.*, 2006, **53**, 201; (*b*) J.-S. Lin, Y.-C. Chen, C.-C. Chen, L. Luo, E. W.-G. Diau and T.-F. Liu, *J. Chin. Chem. Soc.*, 2006, **53**, 1405.